Development of a New Micro Drilling Tool with H-Shaped Chisel Edge

Yue Ma [1], Zhiqiang Liang [1,*], Kun Wan [2], Rongbin Cai [2], Linfeng Yi [2], Jianfei Li [2], Fei Wang [3], Xu Zhao [4], Rui Chen [1] and Xibin Wang [1]

[1] School of Mechanical Engineering, Beijing Institute of Technology, Beijing 100081, China; 15546108005@163.com (Y.M.); 17864307551@163.com (R.C.); cutting0@bit.edu.cn (X.W.)

[2] AECC South Industry Co., Ltd., Zhuzhou 412002, China; wankun0316@163.com (K.W.); rbvxs@163.com (R.C.); yilinfeng@21cn.com (L.Y.); nfgslijianfei@163.com (J.L.)

[3] Inner Mongolia North Heavy Industries Group Corp., Ltd., Baotou 014030, China; wf813517@163.com

[4] Xi'an Institute of Electromechanical Information Technology, Xi'an 710065, China; xu_zhao@sohu.com

* Correspondence: liangzhiqiang@bit.edu.cn; Tel.: +86-10-68911214

Abstract: In order to improve the tool life and micro-hole machining quality, the H-shaped chisel edge micro-drill (HCE-MD) was developed in this paper. The HCE-MD was characterized by the inner edge formed through the chisel edge thinning. In the micro-drilling process, the inner edge can perform positive rake cutting, so the machining area of the workpiece extruded by cutting edge with a negative rake angle is reduced. Based on this, the distribution of rake angle near the chisel edge corner is improved. Then, the HCE-MD was fabricated on the six-axis CNC grinding machine. The grinding process parameters of the micro-drill were optimized based on the orthogonal grinding test and grey relational grade theory. The size and shape accuracy of the micro-drill were controlled by the multi-axis linkage grinding method and the movement-axis micro compensation method. Finally, the 0.25 mm HCE-MD was fabricated with the cutting edge radius of 1.94 μm and the flank surface roughness of 0.25 μm. The drilling performance of HCE-MD was evaluated through comparative drilling experiments. The experimental results show that, compared with common micro drill, the HCE-MD produced lower thrust force and better micro-hole roundness accuracy, and reduced the micro-drill wear on the chisel edge and the flank.

Keywords: micro-drill; chisel edge thinning; tool grinding; drilling performance

1. Introduction

With the development of advanced industry, the micro-hole parts are widely used in aviation, aerospace, medical, electronics, and many other industries [1–4]. These micro-hole parts are generally made of high-temperature alloy, titanium alloy, stainless steel, and other materials, which are difficult to process [5–7]. With the miniaturization of the micro-hole diameter and the increase in the depth diameter ratio, the cutting load, friction, impact, and other working conditions that the tool bears in the drilling process become more complex [8], and the cutting force and cutting temperature are higher, which is more likely to cause tool wear, breakage, and other failures, thus affecting the machining quality of micro-holes [9,10].

At present, the chisel edge (CE) thinning is considered to be an effective means to improve the tool drilling performance. Hanyu et al. [11] applied the CE thinning to the diamond-coated drills to improve the coating debonding phenomenon at the CE of the drill bit caused by excessive cutting load, and determined the optimum angle of thinning by optimizing the rake angle at the CE. Sugita et al. [12] proposed a new drill web shape based on the formation of additional cutting edge by thinning edge, and performed the drilling experiments on SUS304 stainless steel. Experimental results showed that the cutting force decreased by more than 20% compared with a conventional tool, and the circularity

of the drilled hole was improved. Ko and Lee [13] conducted the comparative drilling experiments with different workpiece materials using the X-type cross-edge drill and conventional drill, and concluded that the drill with CE removed or shortened by thinning can reduce the resistance in drilling and improve the hole accuracy. Wang et al. [14] utilized regular drill and thinned drill to process through-holes on printed circuit board (PCB), and found that appropriate CE thinning can decrease the conglutination phenomenon of chips on major flank and the flank wear of drills. The above studies mainly apply the CE thinning method to the conventional size drilling tools with a diameter of more than 1 mm, and some scholars also preliminarily explore the influence of CE thinning on the cutting performance of micro-drills. For example, Guo et al. [15,16] investigated the drilling performance of helical point micro-drill with a distinct CE length and axial rake angle, and found that the micro-holes processed by thinned micro-drills had smaller entrance burrs, lower roundness errors, and more regular shapes compared to normal micro-drill. Liang et al. [17] studied the application of CE thinning on the high-aspect-ratio micro-drill with 0.5 mm diameter, and verified that the micro-deep-hole drilled by the thinned high-aspect-ratio micro-drill has hole-wall roughness and entrance roundness error. Nanbu et al. [18] demonstrated that when machining the micro-hole with a diameter of 0.2 mm and a depth of 4 mm by thinned high-aspect-ratio micro-drill, the thrust force was reduced and the tool life was prolonged. However, the above ground CE structures used in micro-drills are usually simple in structure form and grinding process, such as the cross-shaped and X-shaped CE. At present, there is no general definition and nomenclature for the structure form of CE thinning. The CE thinning designs already in the literature can be divided into four categories: only thinning the CE, thinning the CE and cutting edge, thinning the CE and flank, and simultaneously thinning the above three structures. Although for conventional size drilling tools, the CE thinning method is widely used. However, there is little research on the application of CE thinning to micro-drill. At the same time, due to the low strength and stiffness of the micro-drill, the micro-drill CE is much more difficult to be thinned. Thus, the micro-drill generally adopts a simple form of CE thinning, such as the cross-shaped CE of only thinning the CE [15,17]. Therefore, it is necessary to further explore a new type of thinned CE suitable for micro-drills.

This study innovatively applies the new H-shaped CE structure to the micro-drill to realize the overall improvement of the tool life and micro-machining quality. In this paper, the design, grinding method and drilling performance of the micro-drill with H-shaped chisel edge (HCE-MD) were investigated. The grinding process parameters of the micro-drill were optimized by orthogonal grinding tests and grey relational grade theory, and then the HCE-MD with a 0.25 mm diameter was fabricated based on the multi-axis linkage CNC grinding method and the micro compensation method of motion axis error. On this basis, the micro-hole drilling experiment was carried out on martensitic stainless steel, and the drilling force, drill wear and hole processing quality were measured and analyzed to study the drilling performance of the fabricated micro-drill. The structural design principle and manufacturing method of HCE-MD can provide reference for the development of high-performance micro-drills.

2. Structure Design of the Micro-Drill

The structure of micro-drill tip directly affects the cutting angle in the drilling process, and then affects the cutting performance and tool life. The CE is one of the main structural features of the drill tip. In the process of micro drilling, the CE part has the characteristics of low cutting speed and negative rake angle cutting, so the drilling force generated by the CE often exceeds that at the cutting edge [19], which speeds up the tool wear failure. In addition, the point angle at the CE area is relatively large, resulting in poor centering ability of the micro-drill, which seriously affects the entrance morphology and surface quality of the machined micro-holes. Therefore, it is necessary to reasonably design the geometric structure of the micro-drill CE in order to improve the tool cutting performance.

The HCE-MD with 0.25 mm diameter is developed. As shown in Figure 1, this thinned CE structure effectively reduces the CE length, forms an inner edge at the turning point of the original CE, and forms the structure of secondary flank. The cutting states of cutting edge, each part of the HCE-MD, and the common micro drill (CMD) are shown in Figure 2. The positions A and B are respectively located on the main cutting edge near the outer edge turning point and drill core. From the turning point of the outer edge to the drill core, the tool rake angle gradually changes from positive to negative, the shearing effect of the cutting edge is weakened, but the pushing effect on the workpiece material is enhanced, then the material removal ability is reduced. Position C is located at the CE area. During drilling process, the CE scrapes and extrudes the workpiece material with a great negative rake angle, so the cutting resistance is large. However, HCE-MD forms the inner cutting edge (at position D) for positive rake angle cutting after CE thinning, which improves the distribution of rake angle near the CE corner, thereby reducing the cutting force. At the same time, the secondary flank structure of the HCE-MD can effectively reduce the friction between the micro-drill flank and the hole bottom, and improve the tool centering performance.
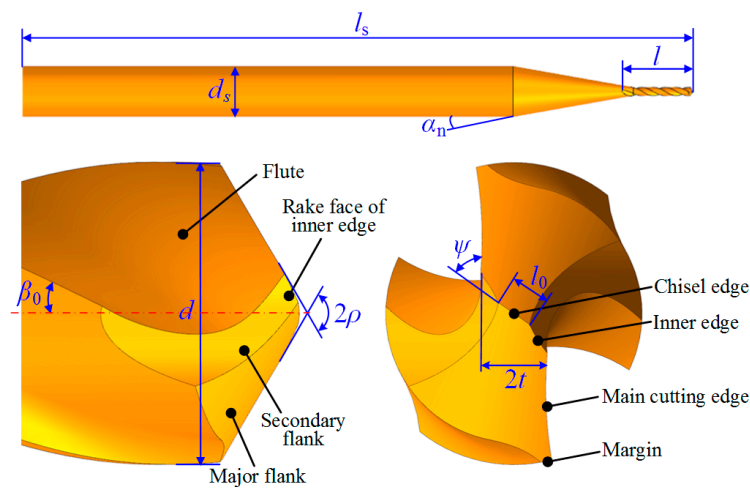
Figure 1. Schematic diagram of the HCE-MD geometric structure.
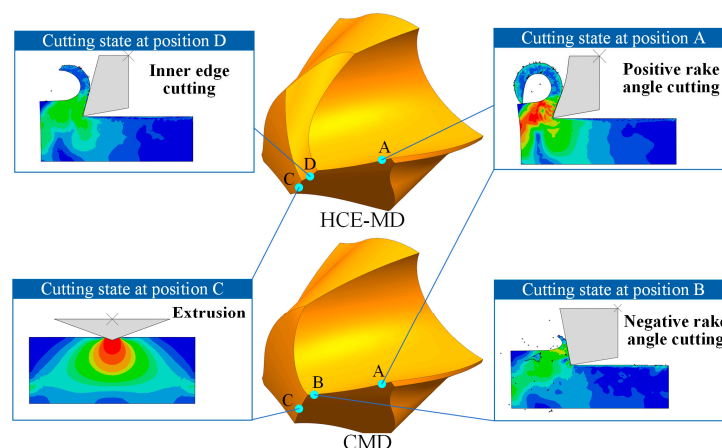
**Figure 2.** Cutting state of micro-drill cutting edge.

3. Experimental Procedure

3.1. Grinding Experiment of HCE-MD

3.1.1. Preparation Conditions

The HCE-MD is fabricated based on the six-axis CNC grinding machine (CNS7d, Makino Seiki Co., Ltd., Tokyo, Japan). Figure 3a shows the configuration of the grinding

machine and the movement of each axis. During the tool grinding process, the drill shank is fixed on A-axis, and the micro-drill can move linearly along the Y-axis and the U-axis, as well as rotate around the A-axis and the W-axis. The grinding wheel can move in a straight line along the X-axis and Z-axis. The geometric structure and installation layout of the grinding wheel for micro-drill grinding are presented in Figure 3b. The main dimensions of single bevel grinding wheel are as follows: wheel diameter D_{w1} = 135 mm, wheel width u_1 = 4 mm, and wheel cone angle η = 45°, while the parallel grinding wheel is selected with wheel diameter D_{w2} = 100 mm, wheel width u_2 = 4 mm. The end face I and cylindrical surface II of the parallel grinding wheel usually participate in the grinding of the tool, while the single bevel grinding wheel uses the cone angle formed by the conical face III and end face IV to finish the grinding of the tool structural features. L_{w1} and L_{w2} represent the distances from the end face of each grinding wheel to the machine base, which are measured by the dial indicator. Both grinding wheels are 2000# vitrified bond diamond grinding wheel, and the micro-drill material is UF12 grade produced manufacturer IMC GROUP with an average grain size of 0.5 μm.
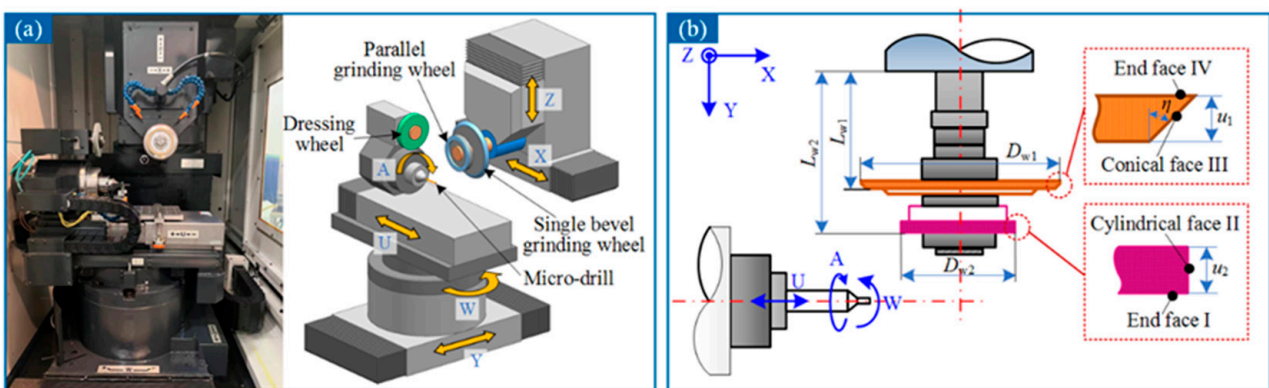
Figure 3. Tool grinding experimental device. (**a**) Structure of tool grinding machine; (**b**) structure and position of grinding wheel.

With the decrease in micro-drill diameter and the increase in length diameter ratio, the rigidity and strength of the micro-drill are significantly reduced, and the tool grinding difficulty increases. At the same time, the influence of the grinding quality on the cutting performance of the micro-drill is more prominent. In order to achieve high-precision and high-quality grinding of the HCE-MD, the optimization test of the tool grinding process is conducted. Based on the orthogonal test method, the orthogonal test of three factors and four levels (as shown in Table 1) is designed with the surface roughness of the micro-drill flank and the cutting edge radius as the optimization indicators.

Table 1. Optimization factor-level table of drill-tip structure parameters.

Factors	Levels	Grinding Speed v_c (m/min)	Feed Rate v_f (mm/min)	Grinding Depth a_p (μm)
	1	1200	300	4
	2	1300	400	8
	3	1400	500	12
	4	1500	600	16

After the experiment, the tool surface roughness and cutting edge radius of the fabricated micro-drill are detected by 3D laser scanning microscope (VK-X100, Keyence Co., Ltd., Japan, Osaka). When measuring the surface roughness of the micro-drill flank, the correction tilt treatment is applied to the flank first. Then the inspection areas of same size are selected on the two flanks, and three roughness profiles (sampling area 30 μm × 30 μm) are measured in each area, as presented in Figure 4a. The average surface roughness

value Ra of the six measurements is then calculated. The measurement method of the micro-drill edge radius is shown in Figure 4b. After collecting the three-dimensional profile of the cutting edge through the laser scanning microscope, the matching VK analysis software is used to obtain the two-dimensional section profile of the cutting edge, then the measurement value of edge radius re is obtained through the three-point fitting method. Three measurement points are selected at the middle position of each main cutting edge, and the average value of six measurements is calculated to represent the edge radius r_e.
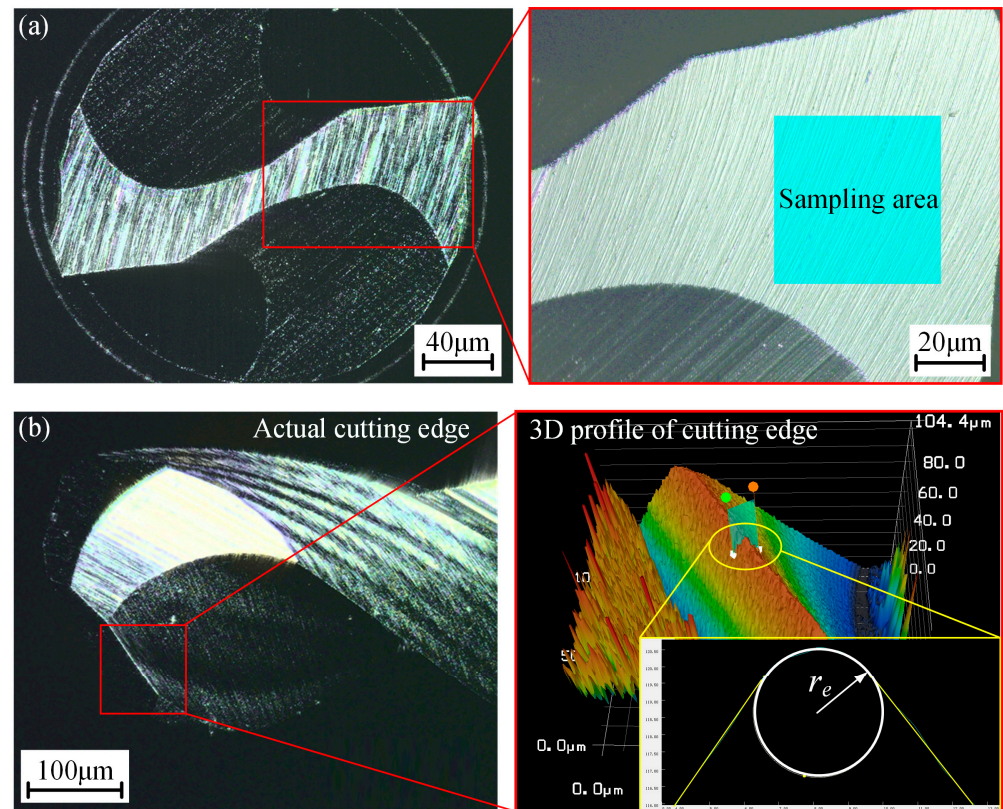
Figure 4. (**a**) Measurement method of the flank roughness; (**b**) measurement method of the micro-drill edge radius.

3.1.2. Grinding Principle

As shown in Figure 5, the fabrication of the HCE-MD mainly includes the following six processes: tip grinding, cylindrical face grinding, flute grinding, edge back grinding, flank grinding, and CE thinning.
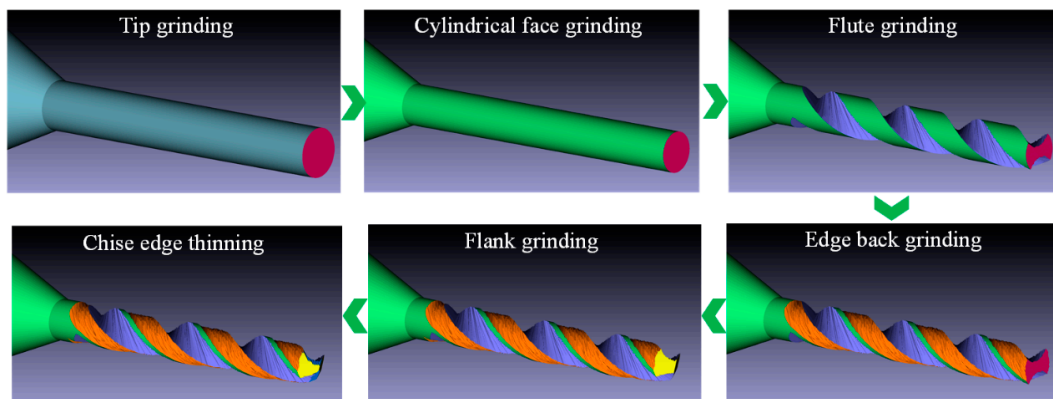

Figure 5. Grinding process of the HCE-MD.

(1) Tip grinding

The surface defects on the tool bar end face are removed through the tip grinding, and the machining schematic diagram is shown in Figure 6a. First, the cut-off position is determined through the three-axis linkage of X-axis, Y-axis, and W-axis. Then the cylindrical surface II of the parallel grinding wheel is fed along the Z-axis to finish cutting off the tip of tool bar. The cutting length of bar tip can be adjusted by Y-axis micro compensation of the grinding machine.
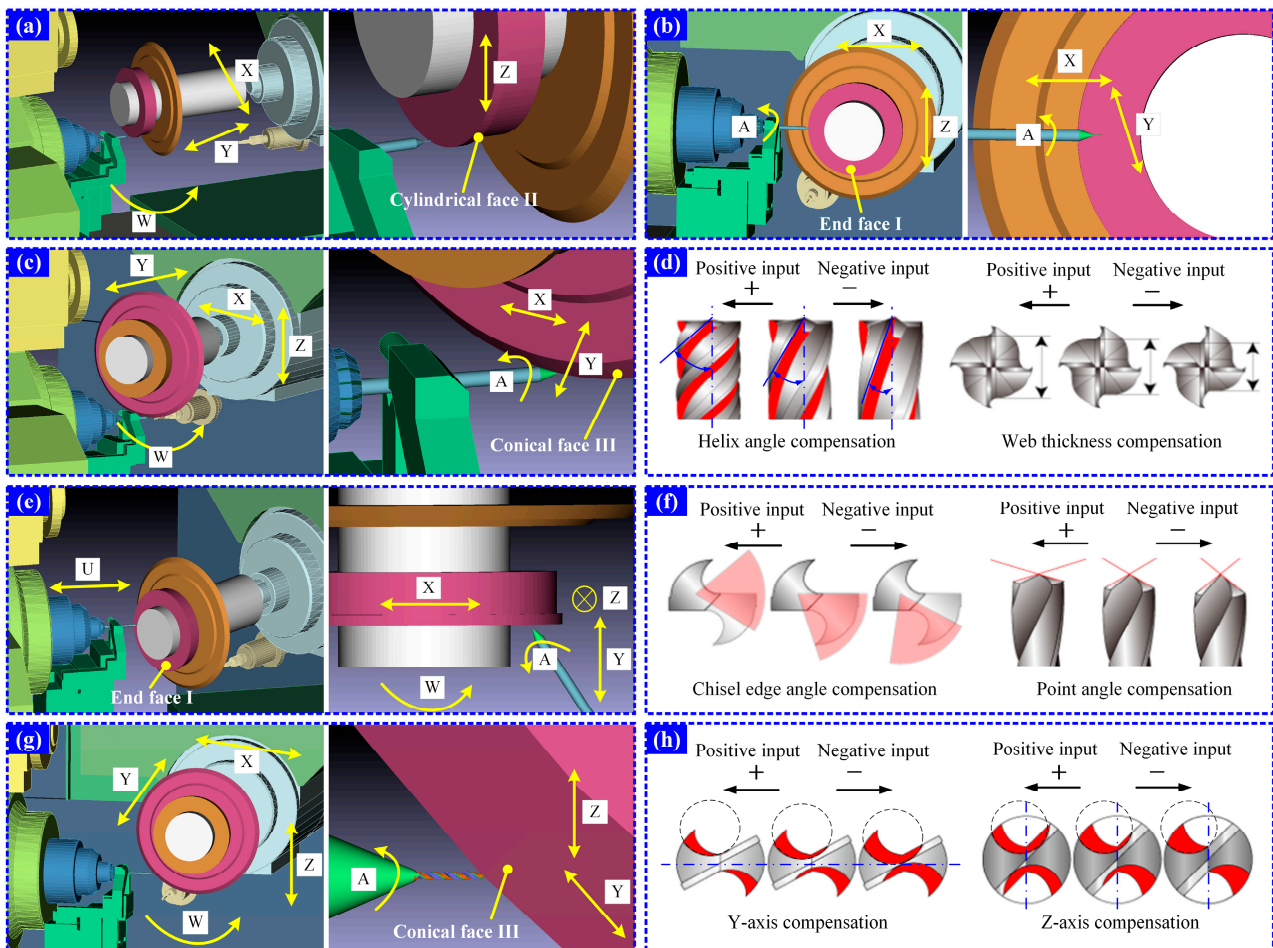
Figure 6. Schematic diagram of machining principle for each process. (**a**) Tip grinding; (**b**) cylindrical face grinding; (**c**) flute grinding; (**d**) micro compensation of flute characteristic parameters; (**e**) flank grinding; (**f**) micro compensation of flank characteristic parameters; (**g**) CE thinning; (**h**) micro compensation of the thinned CE dimension.

(2) Cylindrical grinding for micro-drill margin

This process is used to grind the cylindrical surface where the micro-drill margin is located, and control the tool diameter. The principle of this grinding process is presented in Figure 6b. The grinding machine moves to the initial machining position through X-axis and Z-axis. Then, the end face I of the parallel grinding wheel moves along the X-axis, and the grinding depth is controlled through the Y-axis to reduce the tool diameter to the specified size. The machining errors caused by grinding wheel wear and machine positioning can be corrected by micro adjustment of X-axis and Y-axis.

(3) Flute grinding

As the main structure of drill tip, the flute determines the chip removal ability, strength, and stiffness of the micro-drills. The helix angle and web thickness of the micro-drill are

important parameters to characterize this structure. As shown in Figure 6c, the single bevel wheel moves to the designated position through X-axis and Z-axis, and the tool clamping axis moves through the Y-axis and W-axis to the initial position of the flute grinding. In the grinding process, the X-axis and Y-axis form an interpolation motion to ensure that the tool moves along the U axis direction. At the same time, the A-axis rotates to generate the relative spiral motion between the grinding wheel and micro-drill. The conical face III and end face IV of the grinding wheel jointly complete the grinding of the micro-drill flute. As shown in Figure 6d, the micro compensation of helix angle requires the joint action of X-axis and Y-axis, and the size error of web thickness can be corrected by adjusting the initial position which controlled by Z-axis. The grinding principle of the edge back is the same as that of the flute grinding.

(4)   Flank grinding

The drill tip structure of the cutting edge and CE can be formed by the flank grinding, and the micro-drill flank is affected by the structural parameters such as the point angle and CE angle. In the grinding process, the tool positioning before grinding is completed through the U-axis movement, and then the flank grinding is realized through the five axis linkage of X, Y, Z, A and W axes, using the end face I of the grinding wheel. Based on the grinding principle of the micro-drill flank, when the size of the point angle and CE angle deviates, the CE angle can be corrected by adjusting the A-axis micro compensation, and the point angle can be corrected by W-axis, as shown in Figure 6f.

(5)   Chisel edge thinning

The movement principle of the grinding machine during the CE thinning is shown in Figure 6g. Before machining, the tool is positioned to the grinding position through X, Y, Z, and W axes linkage. Then, the cone angle generated by the intersection of conical face III and end face IV of the single bevel grinding wheel is used to realize the CE thinning. And the thinned CE is obtained through the motion of the Y-axis and Z-axis and the rotation of the A-axis. The dimension error at the CE is mainly compensated by the micro adjustment of Y-axis and Z-axis, as presented in Figure 6h. The Y-axis affects the eccentric position of the CE thinning, and the Z-axis controls the height of the thinned CE.

3.2. Performance Experiment of HCE-MD

As shown in Figure 7, the micro-drilling comparative experiments are carried out on a DMG machining center (DMU80 monoBLOCK, DMG MORI Co., Ltd., Bielfeld, Germany) to validate the drilling performance of the HCE-MD. The geometric morphology of the CMD as the control group is shown in Figure 8. The CMD is fabricated with the same equipment and process as the HCE-MD. Except that its CE length is 70 μm, the other geometric parameters are consistent with the HCE-MD. During the drilling experiment, the high-speed precision spindle (HES801-HSK A63, NAKANISHI Co., Ltd., Kanuma, Japan) is utilized to clamp the micro-drill, which has a runout error of less than 1 μm and can provide the highest speed of 80,000 r/min. The thrust force is measured using a piezoelectric dynamometer (Kistler 9257B, Kistler Instrumente AG, Winterthur, Switzerland), and the workpiece is fixed on the dynamometer through a fixture. A difficult-to-machine material, 9Cr18Mo martensitic stainless steel, is used as the workpiece material in this study, and the experimental parameters are listed in Table 2. Two groups of repeated experiments were carried out under the conditions of each micro-drilling parameter. After the drilling experiment, the micro-hole morphology and tool wear are observed and measured by thermal field emission scanning electron microscope (Quanta 650FEG, FEI Company, Portland, OR, USA) and Keyence laser scanning microscope.
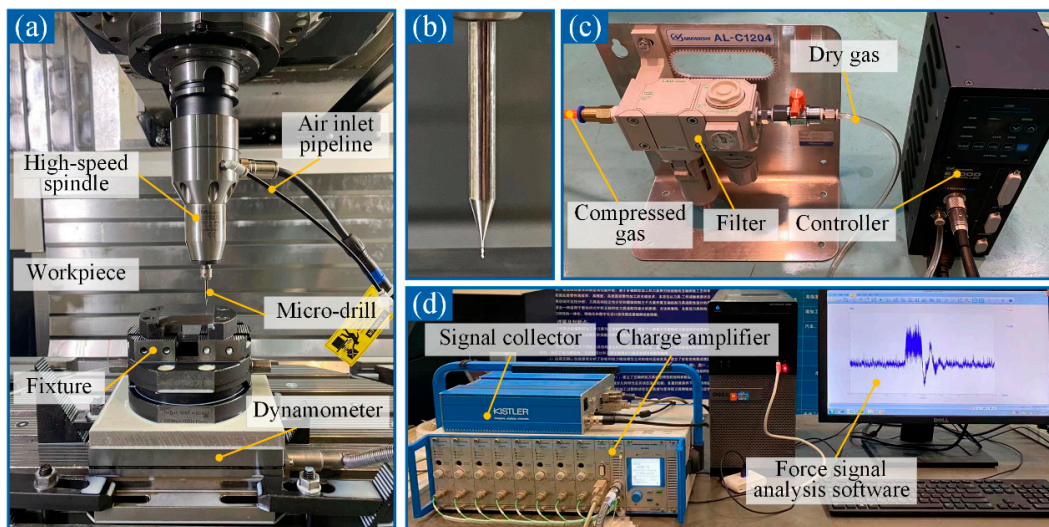
Figure 7. Micro-drilling experimental device. (**a**) Experimental process; (**b**) micro-drill; (**c**) supporting components for high-speed spindle; (**d**) supporting components for dynamometer.
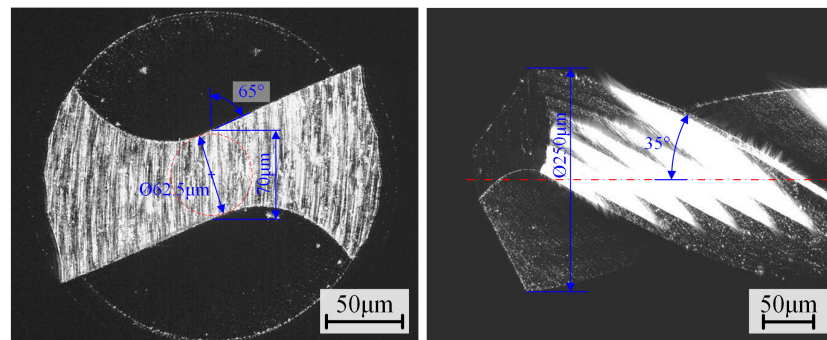
Figure 8. Geometric morphology of the CMD.

Table 2. Experimental parameters of micro-drilling.

Parameters	Values
Spindle speed n (r/min)	10,000, 20,000, 30,000, 40,000, 50,000
Feed rate f (mm/min)	10, 20, 30, 40, 50
Micro-hole diameter (mm)	0.25
Drilling depth (mm)	1.5
Peck drilling depth (mm)	0.03
Coolant condition	Water-based cutting fluid

4. Results and Discussion

4.1. Fabrication and Process Optimization of HCE-MD

The results of the grinding process optimization experiment are shown in Table 3. In order to analyze the comprehensive influence of grinding process parameters on the tool surface roughness and cutting edge radius, the test results shown in Table 3 are processed according to the gray relational optimization method proposed in Reference [20]. First, dimensionless processing is performed on the test results of surface roughness and edge radius through Equation (1).

$$y_i(j) = \frac{x_i(j) - \min\limits_{j} x_i(j)}{\max\limits_{j} x_i(j) - \min\limits_{j} x_i(j)} \tag{1}$$

Table 3. Parameters and results of grinding process optimization test.

Test No.	Factors			Results	
	Grinding Speed v_c (m/min)	Feed Rate v_f (mm/min)	Grinding Depth a_p (µm)	Surface Roughness Ra (µm)	Edge Radius r_e (µm)
1	1200	300	4	0.253	1.97
2	1200	400	8	0.300	2.01
3	1200	500	12	0.357	2.08
4	1200	600	16	0.445	2.15
5	1300	300	8	0.277	1.85
6	1300	400	4	0.269	1.89
7	1300	500	16	0.337	2.05
8	1300	600	12	0.315	2.28
9	1400	300	16	0.292	1.97
10	1400	400	12	0.273	2.21
11	1400	500	4	0.253	1.87
12	1400	600	8	0.265	2.11
13	1500	300	16	0.278	1.96
14	1500	400	12	0.235	1.91
15	1500	500	8	0.265	2.11
16	1500	600	4	0.195	2.01

Here, $x_i(j)$ is the result of the *i*-th evaluation index in the *j*-th test, and $y_i(j)$ is the value of $x_i(j)$ after dimensionless processing, $i = 1, 2$, $j = 1, 2, \ldots, 16$.

Then, the grey relational grade value is calculated by Equations (2) and (3).

$$\xi_i(j) = \frac{\min_i \min_j |y_i^0(j) - y_i(j)| + k \max_i \max_j |y_i^0(j) - y_i(j)|}{|y_i^0(j) - y_i(j)| + k \max_i \max_j |y_i^0(j) - y_i(j)|} \tag{2}$$

$$\gamma_j = \frac{1}{2} \sum_{i=1}^{2} \xi_i(j) \tag{3}$$

Here, $y_i^0(j)$ is the ideal state data of the *i*-th evaluation index, and the ideal state value of surface roughness and edge radius is 0; *k* represents the resolution coefficient, and is set to 0.5.

Through the above calculation, the grey relational grade of grinding quality evaluation indexes under different test conditions are obtained, as illustrated in Table 4. According to the orthogonal test in Table 1, the mean value of grey relational degree under each factor and level is calculated, and then and the influence of grinding parameters on the grey relational grade is obtained, as presented in Figure 9. The process parameters with the highest grey relational grade are the best combination of grinding parameters [21,22]. Therefore, the optimal micro-drill grinding parameters are: grinding speed 1500 m/min, feed rate 300 mm/min, grinding depth 4 µm.

Table 4. Grey relational grade value under different grinding tests.

Test No.	1	2	3	4	5	6	7	8
Grey relational grade	0.662	0.558	0.459	0.375	0.802	0.736	0.493	0.422
Test No.	9	10	11	12	13	14	15	16
Grey relational grade	0.602	0.495	0.799	0.547	0.631	0.770	0.547	0.787
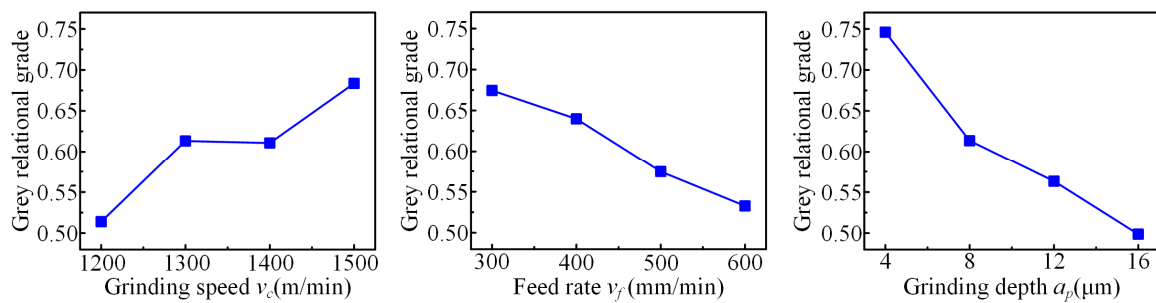
Figure 9. Influence of process parameters on the grey relational grade.

Based on the above grinding principle and the optimized grinding process parameters, the HCE-MD is fabricated (as presented in Figure 10). The overall structure and corresponding geometric parameters of the HCE-MD are shown in Figure 1 and Table 5 respectively. The fabricated micro-drill has the flank surface roughness of 0.25 μm and the cutting edge radius of 1.94 μm.
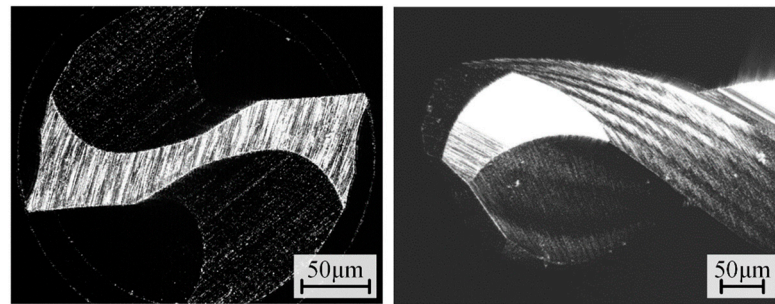

Figure 10. Grinding results of the HCE-MD.

Table 5. Geometric parameters of the HCE-MD.

Parameters	Drill diameter d (μm)	Web thickness $2t$ (μm)	Chisel edge length l_0 (μm)	Point angle 2ρ (°)	Chisel edge angle ψ (°)
Values	250	62.5	20	120	65
Parameters	Flute length l (mm)	Tool whole length l_s (mm)	Tool shank diameter d_s (mm)	Tool neck angle α_n (°)	Helix angle β_0 (°)
Values	1.6	50	3	10	35

*4.2. Drilling Performance of HCE-MD*

4.2.1. Drilling Force

The variation trend of drilling thrust force of different type micro-drills with the micro-hole number and machining parameters is shown in Figure 11. It can be seen that the thrust force rises gradually with the increase in hole number; however, the thrust force of HCE-MD is significantly lower than that of CMD. When machining to the 30th micro-hole, the thrust force of the HCE-MD and CMD are 5.36 N and 10.61 N, and the thrust force of HCE-MD is decreased by 49.5% compared with that of CMD. With the increase of spindle speed and the decrease of feed speed, the thrust force of the two kinds of micro-drills decreases, and the thrust force of HCE-MD is always smaller than that of CMD. This further verifies that the HCE-MD can effectively reduce the drilling thrust force. The inner edge brought by the CE thinning has a significant impact on the rake angle distribution of the HCE-MD. It changes the situation that the micro-drill extrudes the workpiece with a large negative rake angle, forming the inner edge to cut the workpiece with a positive rake angle [23], reducing the workpiece material deformation, thus significantly decreasing the drilling force.
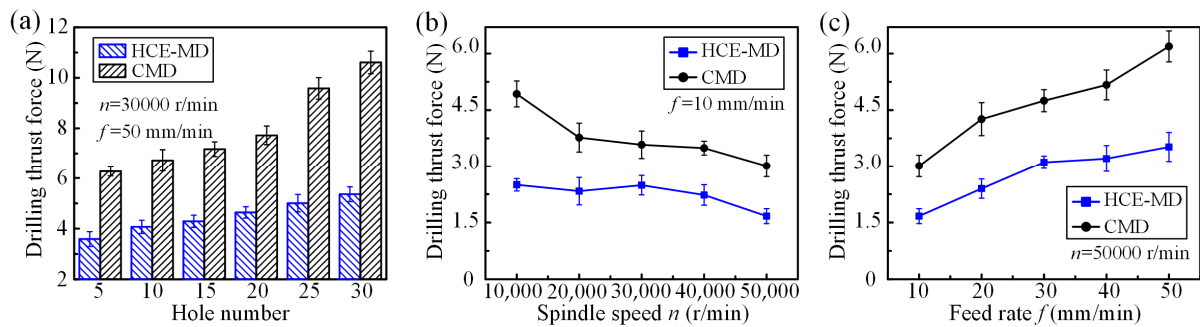
Figure 11. Drilling thrust force of the HCE-MD and CMD. (**a**) Change with hole number; (**b**) change with spindle speed; (**c**) change with feed rate.

4.2.2. Tool Wear

Figure 12 shows the drill tip wear of two type micro-drills after drilling 30 micro-holes. Each segment of cutting edge of HCE-MD and CMD is worn with different degrees, especially the CE. In order to quantitatively analyze the tool wear, the wear width of the micro-drill cutting edge is measured by the VK analysis software of Keyence laser scanning microscope. As for CMD, the maximum wear width of main cutting edge and CE is 15.93 μm and 34.98 μm, and there is a large wear region on the flank. The maximum wear width of the corresponding cutting edge position of the HCE-MD is 15.82 μm and 21.16 μm, and no obvious wear phenomenon is observed on the micro-drill flank. Compared to CMD, the maximum wear width of the CE of HCE-MD is reduced by 39.5%. This can be explained as that, the CE length of the HCE-MD is reduced through the CE thinning, then the machining area of the workpiece extruded by the CE with a negative rake angle is reduced, and the area where the workpiece is cut with the inner edge having a positive rake angle is enlarged. As a result, the drilling force decreases greatly, which leads to a significant reduction in tool wear. At the same time, the new shape of micro-drill flank brought by CE thinning reduces the friction between the flank and workpiece, and avoiding the flank wear.
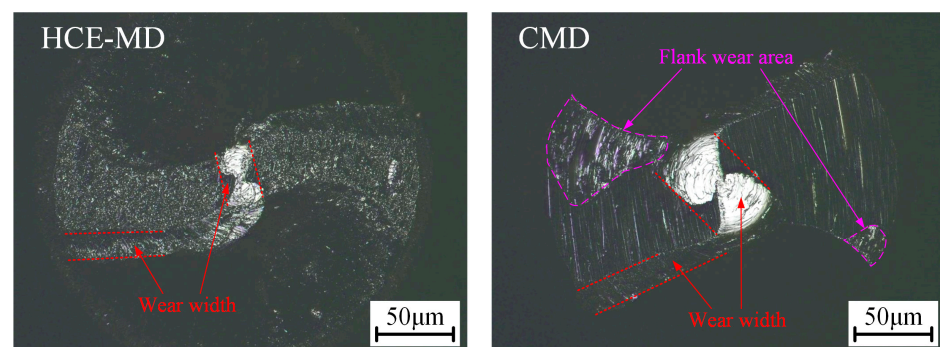

Figure 12. Wear morphology of drill tip.

4.2.3. Machining Quality of Micro-Hole

The entrance morphology of the micro-holes processed by different type micro-drills is shown in Figure 13. Compared with the CMD, the drilling quality of the HCE-MD is more stable. When the CMD is drilling the 30th micro-hole, a large range of edge damage occurs at the hole entrance; however, the micro-holes obtained by HCE-MD still guarantee regular shape of hole entrance. These also correspond to the experimental results of tool wear, which further reflects that the HCE-MD has better wear resistance. The measurement result of micro-hole roundness error is presented in Figure 14. When drilling to the same number of holes, the roundness value of the micro-holes drilled by HCE-MD is much smaller than that of CMD, and increases more slowly with the increase of hole number.

When drilling the 30th micro-hole, the roundness error obtained by the HCE-MD is reduced by 43.8% compared with the CMD. It can be seen from Figure 14b,c that the variation trend of roundness error with spindle speed and feed rate is the same as that of thrust force. When the spindle speed is high and the feed rate is low, although the roundness error of the HCE-MD is always lower than that of the CMD, the roundness error value of the two micro-drills is not much different. Under the process conditions of low spindle speed and high feed speed, the HCE-MD has more significant advantages in micro-hole machining accuracy compared with CMD.
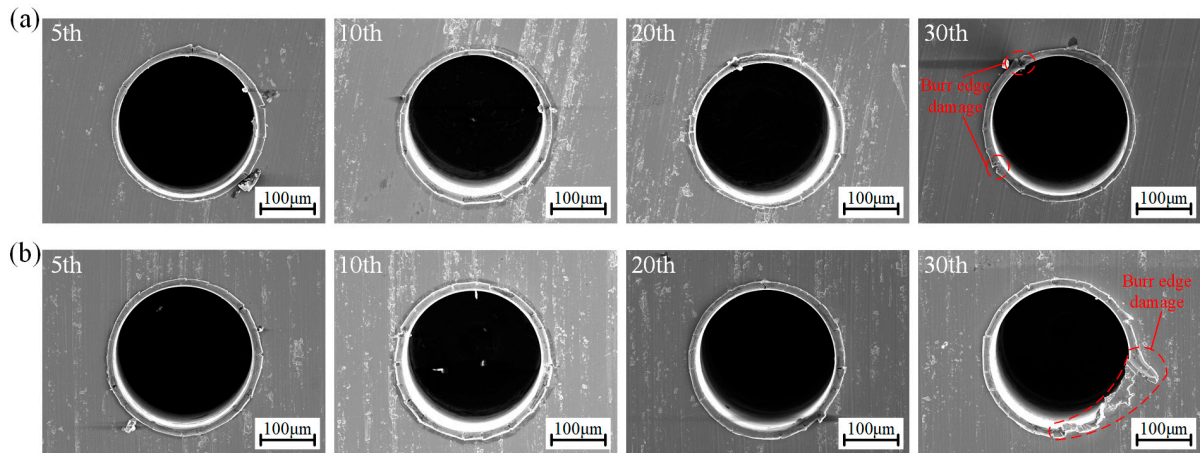
Figure 13. Micro-hole entrance morphology. (**a**) Micro-holes produced by HCE-MD; (**b**) micro-holes produced by CMD.
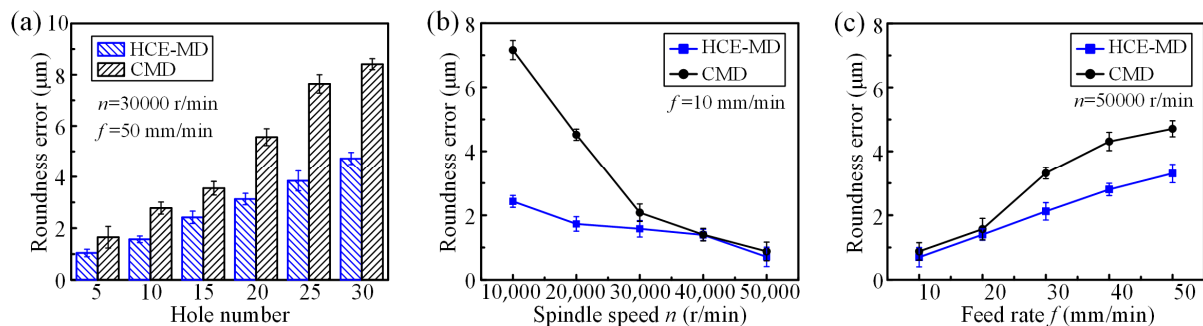
Figure 14. Micro-hole roundness error of the HCE-MD and CMD. (**a**) Change with hole number; (**b**) change with spindle speed; (**c**) change with feed rate.

5. Conclusions

The design and fabrication of the HCE-MD are conducted in this study, and the drilling performance is verified by the comparative drilling tests performed on 9Cr18Mo martensitic stainless steel. By discussing the experimental results from the aspects of thrust force, drill wear, and micro-hole quality, some conclusions can be summarized as follows:

(1) Through the CE thinning, the HCE-MD generates the inner edge and secondary flank structure. The inner edge performs positive rake angle cutting, thus the machining area of the workpiece extruded by the cutting edge with a negative rake angle is reduced, and the distribution of rake angle near the CE corner is improved. The secondary flank effectively reduces the friction between the micro-drill flank and workpiece, and improves the tool-centering performance.

(2) Through orthogonal grinding test and grey relational grade theory, the optimized grinding process parameters of HCE-MD flank are grinding speed 1500 m/min, feed rate 300 mm/min, grinding depth 4 μm. On this basis, the HCE-MD with a 0.25 mm

diameter is fabricated. The fabricated micro-drill has the cutting edge radius of 1.94 μm and the flank surface roughness of 0.25 μm.

(3) Compared with CMD, HCE-MD produces less thrust force and better micro-hole roundness accuracy, and can reduce the micro-drill wear on CE and the flank. Therefore, the machining quality of micro-hole and the tool life are improved. When drilling the 30th micro hole, the thrust force, roundness error, and CE wear width of the HCE-MD are severally reduced by 49.5%, 43.8%, and 39.5%.

The novelty of this study lies in the application of the new CE structure to the micro-drill, which can realize the comprehensive improvement of the service life and micro-machining quality of the micro-drill. In this way, we anticipate that our research will support the high-precision and high-efficiency machining of micro-deep-holes in difficult-to-machine materials, and lead to potential applications in the fabrication of precision microstructure parts. Our future work will focus on optimizing the drill-tip structure parameters of the HCE-MD to further improve its drilling performance.

Author Contributions: Conceptualization, Y.M. and R.C. (Rui Chen); methodology, Y.M.; validation, Y.M., L.Y. and R.C. (Rongbin Cai); investigation, Y.M. and K.W.; resources, F.W. and X.Z.; writing—original draft preparation, Y.M. and R.C. (Rui Chen); writing—review and editing, Y.M. and Z.L.; visualization, Y.M.; supervision, J.L.; project administration, Z.L.; funding acquisition, X.W. All authors have read and agreed to the published version of the manuscript.

Institutional Review Board Statement: Not applicable.

Informed Consent Statement: Not applicable.

Data Availability Statement: The data presented in this study are available within the article.

Conflicts of Interest: The authors declare no conflict of interest.

References

1. Hasan, M.; Zhao, J.W.; Jiang, Z.Y. A review of modern advancements in micro drilling techniques. *J. Manuf. Process.* **2017**, *29*, 343–375. [CrossRef]
2. Wang, M.H.; Zhang, Y.B.; He, Z.W.; Peng, W. Deep micro-hole fabrication in EMM on stainless steel using disk micro-tool assisted by ultrasonic vibration. *J. Mater. Process. Technol.* **2016**, *229*, 75–483. [CrossRef]
3. Leo Kumar, S.P.; Jerald, J.; Kumanan, S.; Prabakaran, R. A review on current research aspects in tool-based micromachining processes. *Mater. Manuf. Process.* **2014**, *29*, 291–337. [CrossRef]
4. Koklu, U.; Basmaci, G. Evaluation of tool path strategy and cooling condition effects on the cutting force and surface quality in micromilling operations. *Metals* **2017**, *7*, 426. [CrossRef]
5. Huang, S.F.; Liu, Y.; Li, J.; Hu, H.X.; Sun, Y. Electrochemical discharge machining micro-hole in stainless steel with tool electrode high-speed rotating. *Mater. Manuf. Process.* **2014**, *29*, 634–637. [CrossRef]
6. Swain, N.; Kumar, P.; Srinivas, G.; Ravishankar, S.; Barshilia, H.C. Mechanical micro-drilling of nimonic 80A superalloy using uncoated and TiAlN-coated micro-drills. *Mater. Manuf. Process.* **2017**, *32*, 1537–1546. [CrossRef]
7. Zai, P.H.; Tong, J.L.; Liu, Z.Q.; Zhang, Z.P.; Song, C.S.; Zhao, B. Analytical model of exit burr height and experimental investigation on ultrasonic-assisted high-speed drilling micro-holes. *J. Manuf. Process.* **2021**, *68*, 807–817. [CrossRef]
8. Kudla, L. Influence of feed motion features on small holes drilling process. *J. Mater. Process. Technol.* **2001**, *109*, 236–241. [CrossRef]
9. Khadtare, A.N.; Pawade, R.S.; Joshi, S. Surface integrity studies for straight and inclined hole in micro-drilling of thermal barrier coated Inconel 718: A turbine blade application. *Precis. Eng.* **2020**, *66*, 166–179. [CrossRef]
10. Kim, D.W.; Lee, Y.S.; Park, M.S.; Chu, C.N. Tool life improvement by peck drilling and thrust force monitoring during deep-micro-hole drilling of steel. *Int. J. Mach. Tools Manuf.* **2009**, *49*, 246–255. [CrossRef]
11. Hanyu, H.; Kamiya, S.; Odagi, H.; Murakami, Y.; Saka, M. Development of high performance diamond-coated drills for cutting high silicon aluminum alloy. *Thin Solid Films* **2002**, *413*, 139–146. [CrossRef]
12. Sugita, N.; Oshima, M.; Kimura, K.; Arai, G.; Arai, K. Novel drill bit with characteristic web shape for high efficiency and accuracy. *CIRP Ann.-Manuf. Technol.* **2018**, *67*, 69–72. [CrossRef]
13. Ko, L.; Lee, J.K. Analysis of burr formation in drilling with a new-concept drill. *J. Mater. Process. Technol.* **2001**, *113*, 392–398. [CrossRef]

14. Wang, X.; Zheng, X.H.; An, Q.L.; Chen, M. Experimental investigation on drilling PCB through-holes. *Adv. Mater. Res.* **2012**, *426*, 56–59. [CrossRef]
15. Guo, H.X.; Liang, Z.Q.; Wang, X.B.; Zhou, T.F.; Jiao, L.; Teng, L.L.; Shen, W.H. Influence of chisel edge thinning on helical point micro-drilling performance. *Int. J. Adv. Manuf. Technol.* **2018**, *99*, 2863–2875. [CrossRef]
16. Liang, Z.Q.; Guo, H.X.; Wang, X.B.; Ma, Y.; Zhou, T.F.; Sun, X.F.; Jiang, L.K. Influence of chisel edge axial rake angle on the drilling performance of helical point micro-drill. *Int. J. Adv. Manuf. Technol.* **2020**, *107*, 2137–2149. [CrossRef]
17. Liang, Z.Q.; Ma, Y.; Chen, J.J.; Li, Y.; Ma, D.; Cao, Y.X.; Cai, R.B.; Guo, H.X.; Wang, X.B. Research on drilling performance of high-aspect-ratio micro-drill with thinned chisel edge. *J. Mech. Eng.* **2021**, *57*, 244–252.
18. Nanbu, Y.; Ochiai, K.; Horio, K.; Kaneko, J.; Watanabe, T.; Matsuda, S. Influence on rake angle of chisel edge in high-aspect-ratio microdrilling. *J. Jpn. Soc. Precis. Eng.* **2011**, *77*, 713–717. [CrossRef]
19. Paul, A.; Kapoor, S.G.; DeVor, R.E. A chisel edge model for arbitrary drill point geometry. *J. Manuf. Sci. Eng.* **2005**, *127*, 23–32. [CrossRef]
20. Tzeng, C.J.; Lin, Y.H.; Yang, Y.K.; Jeng, M.C. Optimization of turning operations with multiple performance characteristics using the taguchi method and grey relational analysis. *J. Mater. Process. Technol.* **2009**, *209*, 2753–2759. [CrossRef]
21. Zhan, Z.B.; Li, L.; He, N.; Shrestha, R. An experimental study on grinding parameters for manufacturing PCD micro-milling tool. *Int. J. Adv. Manuf. Technol.* **2014**, *73*, 1799–1806. [CrossRef]
22. Du, Y.C.; Liang, Z.Q.; Ma, Y.; Su, Z.P.; Chen, R.; Zhou, T.F.; Wang, X.B. Development of PCBN micro ball-end mill with multi-edge and spherical flank face. *J. Manuf. Process.* **2022**, *84*, 424–434. [CrossRef]
23. Lin, P.D.; Tzeng, C.S. New method for determination of the pose of the grinding wheel for thinning drill points. *Int. J. Mach. Tools Manuf.* **2007**, *47*, 2218–2229. [CrossRef]